Detectability in computed tomographic images

Kenneth M. Hanson

University of California, Los Alamos Scientific Laboratory, Los Alamos, New Mexico 87545

(Received 2 November 1978; accepted for publication 7 May 1979)

The detection limitations inherent in statistically limited computed tomographic (CT) images are described through the application of signal detection theory. The detectability of large-area, low-contrast objects is shown to be chiefly dependent upon the low-frequency content of the noise power spectral density. For projection data containing uncorrelated noise, the resulting ramplike, low-frequency behavior of the noise power spectrum of CT reconstructions may be conveniently characterized by the number of noise-equivalent x-ray quanta (NEQ) detected in the projection measurements. The NEQ for a given image may be determined either from a measurement of the noise power spectrum or from the noise granularity computed with an appropriate weighting function. A measure of the efficiency of scanner dose utilization is proposed which compares the average dose to that required by an ideal scanner to obtain the same NEQ.

I. INTRODUCTION

The introduction of the x-ray computed tomographic (CT) scanner[1] to medical imaging has made it feasible to detect the presence of lesions of very low contrast.[2] A dramatic improvement in detectability over previous imaging techniques was made possible through the following innovations: (1) The noise in the reconstructed CT images was significantly reduced through the use of efficient detectors and electronic processing techniques thereby permitting relatively efficient utilization of the radiation dose. (2) The images could be displayed with variable contrast thus overcoming the minimum contrast threshold of the human observer. (3) The CT reconstruction process almost completely eliminated the superposition of various anatomical structures, leading to the reduction of "structural" noise.

Riederer, Pelc, and Chesler[3] have pointed out that uncorrelated statistical noise in the projection data will lead to the unique correlations in the CT reconstruction noise. The presence of these correlations in the images of a commercial CT scanner has been substantiated.[4] Furthermore, these correlations may be altered to some extent by the reconstruction algorithm used in a specific scanner. Conventional summary measures of noise[5] cannot be used directly to characterize CT noise. Signal detection theory will be used in this paper to investigate the large-area, low-contrast detection capabilities inherent in CT images. This will lead to methods which provide a measure of the density sensitivity appropriate to CT noise. It should be noted that the approach taken here may be readily extended to images containing noise with characteristics other than those found in CT images. When images containing conventional uncorrelated (white) noise are analyzed, the conventional figures-of-merit are obtained.[6]

The restriction in this paper to the detection of objects with large area is appropriate to the study of noise properties since it eliminates the influence of the MTF and, what may be equally significant, the discrete representation of the CT image. The results presented here are directly applicable to the clinical problem of the detection of lesions of moderate size, >10-mm-diam, and low contrast, <1%. The detection theory approach presented may be extended to the problem of the detection of smaller objects.

It is hoped that ultimately a model of the detection system of the human observer might be incorporated into a complete description of signal detection in images. CT noise is interesting from this point of view since it provides us with a new type of noise with which to explore the human detection system. Thus psychophysical tests with CT noise might well lead to a new understanding of how we interpret images.

In Sec. II we review the derivation of the noise power spectral density for CT reconstructions and introduce the notion of number of noise-equivalent quanta (NEQ) used to form a CT image. The use of noise granularity in describing CT noise is considered in Sec. III. Section IV outlines the concepts of signal detection theory and their implications for CT reconstructions. In Sec. V we discuss methods which may be used to compare the large-area, low-contrast detection capabilities of different CT scanners. Concluding comments are made in Sec. VI.

II. PROPERTIES OF CT NOISE

The statistical limitations which arise in x-ray computed tomography (CT) due to the counting statistics of the detected x rays have been discussed by numerous authors.[7–14] Furthermore, correlation in CT noise was predicted by Tanaka and Iinuma[8] some time ago. The effect of this correlation on the rms deviation of the mean for averages taken over various-sized areas was first pointed out by Riederer, Pelc, and Chesler.[3] This led Hanson[15] to speculate that the detection of objects in CT reconstructions would be affected by these correlations.

The noise power spectral density may be used to characterize the properties of the noise in images. We will give a brief derivation of the noise power spectral density for CT reconstructions.[15,16] The noise power spectral density S of an image is defined[17] as

 0094-2405/79/050441-11$01.20 © 1979 Am. Assoc. Phys. Med.

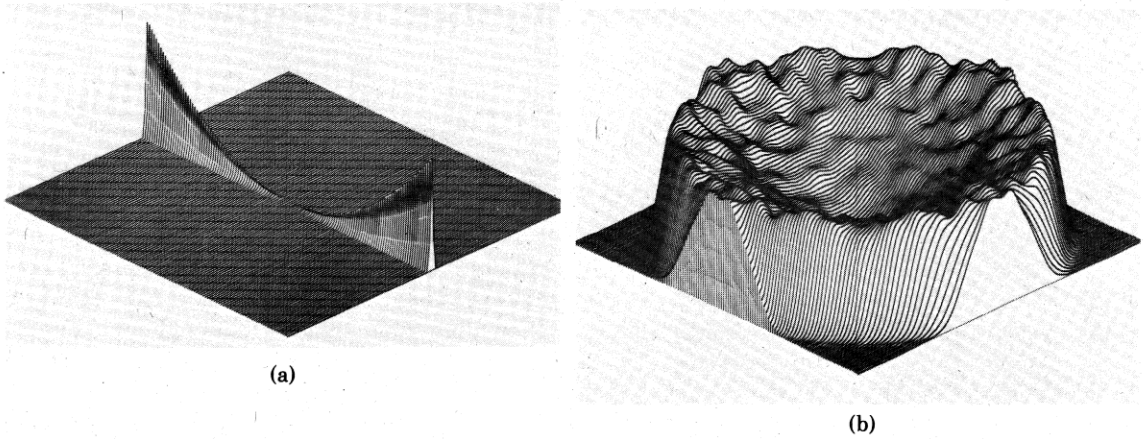

FIG. 1. Noise power spectral density distributions in two-dimensional frequency space, (a) for a single projection a 0° and, (b) for the complete reconstruction.

(a) (b)

$$S(f_x,f_y) = \frac{1}{A}\left\langle \left| \iint_A dxdy\, r(x,y) e^{-2\pi i(xf_x+yf_y)} \right|^2 \right\rangle, \quad (1)$$

where $r(x,y)$ is the reconstruction image containing only noise and the brackets indicate an ensemble average to be carried out over all such noisy images. A is the area over which $r(x,y)$ is defined. For the moment we will consider the filtered backprojection reconstruction algorithm[7] applicable to a planar geometry in which the projections are obtained along parallel lines. The corrective filter to be applied to the projection $p(x)$ is of the form

$$G(f) = |f| H(f). \quad (2)$$

In the limit as f approaches zero frequency, $H(f)$ must approach unity to obtain a reconstruction with the proper normalization. The contribution to $S(f_x,f_y)$ from the backprojection of a single filtered noisy projection will be along a spoke with the radial frequency dependence

$$|f|^2 |H(f)|^2 S_p(f), \quad (3)$$

where S_p is the noise power spectrum for the projection. Figure 1(a) shows the contribution to $S(f_x,f_y)$ from a single projection containing white (S_p = constant) noise for $H(f) = 1$.

Suppose that the complete reconstruction is performed using m projections taken at equally spaced angles covering from 0 to π each with the same S_p. If the projections are statistically independent, it follows from Eq. (1) that the resulting S is merely the sum of the contributions from each projection. The net result is

$$S(f) = \frac{m}{f\pi}\left(\frac{\pi}{m}\right)^2 |f|^2 |H(f)|^2 S_p(f)$$
$$= \frac{\pi}{m} |f|\, |H(f)|^2 S_p(f), \quad (4)$$

where $m/f\pi$ is the spoke density at radial frequency f and π/m is the proper normalization factor for the reconstruction. Figure 1(b) shows the calculated noise power spectrum for a 256 × 256 reconstruction ($H = 1$) from 300 projections which contained simulated white noise. The technique used to calculate S is described in the Appendix for $L = 32$ and $N_{aug} = 128$. The bumpiness in Fig. 1(b) arises from the limited statistical accuracy attained in the estimation of S from a single reconstruction. Figure 1(b) emphasizes the two dimensional nature of S. The radial dependence of S given by Eq. (4) has been verified for simulated reconstructions.[15,16]

The noise variance in the reconstruction image is given by Parseval's relation as the total power

$$\sigma_r^2 = \frac{1}{A}\iint dxdy\, |r(x,y)|^2 = \iint df_x df_y\, S(f_x,f_y)$$
$$= \frac{\pi}{m}\int_0^{2\pi} d\theta \int_0^{f_N} df f^2 |H(f)|^2 S_p(f), \quad (5)$$

where f_N is the Nyquist frequency implied by the assumed bandlimited nature of the projection data. If the projection data are obtained from equally spaced, uncorrelated measurements,

$$S_p(f) = \begin{cases} a\sigma_p^2 & |f| \le f_N \\ 0 & |f| > f_N \end{cases} \quad (6)$$

where a is the spacing between the projection measurements whose variance is σ_p^2 and $f_N = (2a)^{-1}$. The resulting variance in the reconstruction[7] may be conveniently written as

$$\sigma_r^2 = \frac{\sigma_p^2}{m\, a^2} K_{\text{noise}}^2, \quad (7)$$

where

$$K_{\text{noise}}^2 = \frac{\pi^2}{4f_N^3}\int_0^{f_N} df f^2 |H(f)|^2. \quad (8)$$

The noise coefficient K_{noise} defined by Eq. (7) is a dimensionless quantity which describes the propagation of the noise inherent in a particular reconstruction algorithm. Equation (8) allows one to calculate K_{noise} for the filtered backprojection algorithm when the reconstruction coordinates (x,y) are continuous. For example, for $H = 1$, $K_{\text{noise}} = \pi/\sqrt{12} = 0.907$, and for $H = \text{sinc}^2(\pi f/2f_N)$, $K_{\text{noise}} = 0.568$. However, care must be taken in using Eq. (8) to calculate K_{noise}, in particular when x and y represent discrete variables.

$|H(f)|$ may be thought of as the modulation transfer function (MTF)[17] associated with the reconstruction algorithm. It is interesting to note that when linear interpolation is used to interpolate between the sample points in the projection, the result is to introduce a factor of $\text{sinc}^2(\pi f/2f_N)$ to H. However, no such factor occurs when bandlimited interpolation is used. It should be realized that the complete system MTF is the product of several contributing MTF's, and $H(f)$ is only one of these. For example, another contri-

bution is that which arises from the finite width of the radiation beam used to measure the projections.

Let us consider the specific case of statistically limited x-ray computed tomography. Each projection measurement is determined from the ratio of the number of transmitted x rays N, to the number that would be detected if no object were present N_0,

$$p = \int r\,dx = -\ln\left(\frac{N}{N_0}\right). \tag{9}$$

The statistical uncertainty (noise) in each measurement is readily found to be

$$\sigma_p = \frac{1}{\sqrt{N}}, \tag{10}$$

provided $N_0 \gg N$. If approximately the same number of x rays are detected in each projection measurement, we obtain from Eqs. (4) and (6) the noise power spectrum

$$S(f) = \frac{\pi|f|\,|H(f)|^2 a}{mN} \tag{11}$$

We define the number of equivalent quanta (NEQ) as the total number of x rays detected per unit distance along the projections.

$$\mathrm{NEQ} = \frac{mN}{a}, \tag{12}$$

whereby

$$S(f) = \frac{\pi|f|\,|H(f)|^2}{\mathrm{NEQ}}. \tag{13}$$

Recalling that H must approach unity as f goes to zero, the noise power spectrum has the limit

$$\lim_{f\to 0} S(f) = \frac{\pi|f|}{\mathrm{NEQ}}. \tag{14}$$

Also, the noise variance in the reconstruction is

$$\sigma_r^2 = \frac{K^2_{\mathrm{noise}}}{a^3\mathrm{NEQ}}. \tag{15}$$

Our definition of NEQ differs from that proposed by Wagner, Brown, and Pastel[18] in that it includes the number of projections m and thus refers to the total effective number of detected quanta per unit length rather than to the number of per unit length in each projection. It will be shown in Sec. IV that NEQ may be used to characterize the large-area, low-contrast detectability of CT images.

It should be noted that the ramp-like nature of S near $f = 0$ is a general property of reconstructions in which the noise in the projection data is uncorrelated. Thus, any measure of the slope of S near the origin might be viewed as equivalent to the use of NEQ. NEQ has the advantage of possessing a physical interpretation when applied to x-ray computed tomography.

The noise autocorrelation function $C(x,y)$ may be used as an alternative description of the noise properties. Since it is just the inverse Fourier transform of S

$$C(x,y) = \iint df_x\,df_y\,S(f_x,f_y)e^{-2\pi i(xf_x+yf_y)}. \tag{16}$$

C provides equivalent information about the noise as does S. It may be shown that the ramp-like nature of S for uncorrelated projection noise implies that the asymptotic dependence of C is $-\rho^{-3}$ where ρ is the radial distance. Thus it is said that CT noise contains long-range negative correlations.

A word about units is appropriate. We see from Eq. (9) that the projection p is dimensionless and that the reconstructed quantity r has units of $(\text{length})^{-1}$. Then, Eq. (1) indicates that S will be dimensionless. From Eq. (14), NEQ has the same units as frequency f, $(\text{length})^{-1}$, which is consistent with its definition as the number of quanta per unit length, Eq. (12).

For ease of notation the formulae developed in this section have been based on continuous variables and continuous Fourier transforms. They may readily be extended to discrete variables appropriate to the practical situation, where r is determined for picture elements (pixels) at discrete values of x and y. The use of continuous variables is a good approximation if the dimensions of the objects considered are both much larger than the pixel width, say greater than 5 pixels, and much smaller than the full image width. This is precisely the realm of concern in the present paper for objects referred to as "large-area."

III. NOISE GRANULARITY

Several measures of the granular nature of the image noise have been used in the past to investigate film noise.[17] Here we shall define the noise granularity as

$$G(A) = \sigma_A\sqrt{A}, \tag{17}$$

where σ_A is the rms deviation of the mean noise averaged over an area A. G is Selwyn's granularity coefficient[19] divided by $\sqrt{2}$. We wish to extend the above definition to include weighted means. Consider the weighted mean of an image $r(x,y)$

$$m_A(x,y) = \iint dx'dy'\,r(x-x',y-y')w(x',y'), \tag{18}$$

where the weights $w(x,y)$ are normalized to unity:

$$\iint dxdy\,w(x,y) = 1. \tag{19}$$

Then σ_A^2 is given by the variance in m_A. The effective area is defined

$$A = [\iint dxdy\,w^2(x,y)]^{-1}, \tag{20}$$

so that G is independent of A for uncorrelated noise.

The weighted mean $m_A(x,y)$ defined by Eq. (18) may be thought of as a smoothed version of the original image r where w is the smoothing function. The Fourier transform of m_A is therefore equal to the product of the Fourier transforms of r and w. It can be shown that the variance of m_A may be written as

$$\sigma_A^2 = \iint df_x\,df_y\,S(f_x,f_y)W^2(f_x,f_y), \tag{21}$$

where S is the noise power spectrum of r and W is the Fourier transform of the weighting function w. Then G may be expressed in terms of frequency variables as

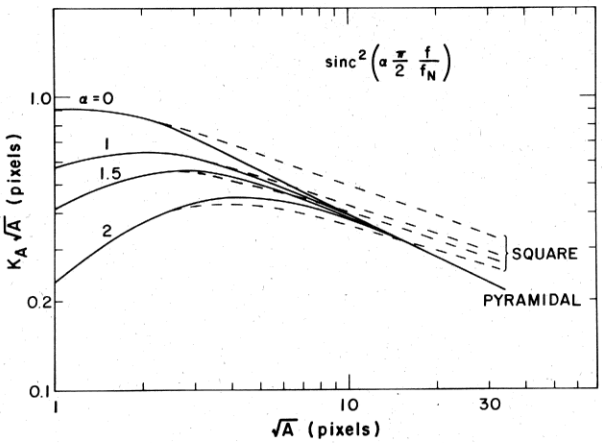

FIG. 2. The noise granularity coefficients for several sinc^2 reconstruction filters. The dashed curves are for constant weights within a square region. The solid curves are calculated using a pyramidal weighting function.

$$G = \left[\frac{\iint df_x\, df_y S\, W^2}{\iint df_x\, df_y\, W^2}\right]^{1/2}. \tag{22}$$

It is observed that although G is related to S, S should be considered as a more fundamental measure of the noise characteristics than G. However, there may be some merit in the use of G since it may be easier to calculate G in real space than to calculate S. Moreover, as will be shown in Sec. IV, G is directly related to the signal-to-noise ratio (optimized for white noise) for the detection of large-area objects. Thus, G may be more closely related to the detection capabilities of an image than S.

In order to demonstrate the expected dependence of G upon A for CT noise, let us define an averaged noise coefficient K_A in a manner similar to Eqs. (7) and (8):

$$\sigma_A^2 = \frac{\sigma_p^2}{m\, a^2} K_A^2 \tag{23}$$

$$K_A^2 = \frac{\pi^2}{4 f_N{}^3} \int_0^{f_N} df\, f^2 |H(f)|^2 |W(f)|^2 \tag{24}$$

Thus

$$G = \frac{\sigma_p}{a\sqrt{m}} K_A \sqrt{A}. \tag{25}$$

The A dependence of $K_A\sqrt{A}$ is shown in Fig. 2 for a family of filters of the form $H = \mathrm{sinc}^2(\alpha\pi f/2f_N)$. The curves in Fig. 2 are calculated using the discrete equivalent of Eqs. (20) and (24) under the assumption that a is both the pixel width and the projection sample spacing. Two different weighting functions are used. The dashed curves are computed using a constant weighting throughout a square of area A. It is observed that the behavior of these curves for large $\sqrt{A}$ is affected by the amount of high frequency filtering. This interesting result is easily understood since aside from an oscillatory behavior, W^2 asymptotically falls off as f^{-2}, just cancelling the f^2 factor in the integral in Eq. (24) and leaving the high frequency contributions of H^2.

The solid curves in Fig. 2 are the results for a pyramidal weighting function which for even n is given by

$$w(i,j) = \begin{cases} C\left|\dfrac{n+1}{2} - i\right|\left|\dfrac{n+1}{2} - j\right| & 1 \le i,j \le n \\ 0 & \text{otherwise.} \end{cases} \tag{26}$$

C is fixed by Eq. (19) and A is calculated from Eq. (20). For $m \gg 1$, $A = 3n^2/4$. The curves for pyramidal weighting converge rapidly as $\sqrt{A}$ increases. This is a result of the more rapid fall off of W^2 than for square weighting. Thus, pyramidal weighting has the advantage that, for large $\sqrt{A}$, it provides a better measure of the low frequency behavior of S.

Equation (22) may be used to derive a relationship between G and the low frequency behavior of S, as characterized by NEQ [Eq. (14)]. A gaussian weighting function will be assumed for the moment:

$$w(\rho) = \frac{1}{2\pi\rho^2} e^{-\rho^2/2\sigma^2} \tag{27}$$

$$W(f) = e^{-2\pi^2\sigma^2 f^2}. \tag{28}$$

Then the effective area is $A = 4\pi\sigma^2$. Evaluation of Eq. (22) yields

$$GA^{1/4} = \left(\frac{\pi}{2\,\mathrm{NEQ}}\right)^{1/2} = \frac{1.253}{\sqrt{\mathrm{NEQ}}}. \tag{29}$$

This formula holds for all values of A for an "exact" reconstruction in continuous variables, provided $\sqrt{A}$ is much larger than the width of the spatial resolution function. However, for discrete variables it can only be approximately correct for $A \gg$ pixel area. Equation (29) is useful since asymptotically it is approximately valid for a variety of weighting functions, provided the corresponding $W(f)$ falls off faster than f^{-1}. For example, above $\sqrt{A} \approx 10$ pixels the curves in Fig. 2 for a pyramidal weighting function approximately satisfy Eq. (29) with the constant changed to 1.240. Thus, the noise granularity function G may be used to determine NEQ if calculated for appropriate weighting functions.

IV. SIGNAL DETECTION THEORY

Signal detection theory[20,21] may be used to develop a measure of the detectability of objects in CT images. To simplify matters we will only consider the binary decision problem in which the decision is to be made whether or not a specific object is present at a specific location. The binary decision case may be extended to the multiple decision situation[22,23] or to the problem of the search for objects within an image.[5]

We will briefly review the procedure[6] used to construct the best decision criterion, which is referred to as the "optimum receiver." The first step is to construct a decision function ψ, which is based on the relative likelihood that the image in question contains the object or not. In order to reach the optimum decision, ψ will include the known correlation properties of the noise. If the noise is gaussian distributed (but not necessarily uncorrelated), then the relative frequency of occurrence of different values of ψ for a given type of image

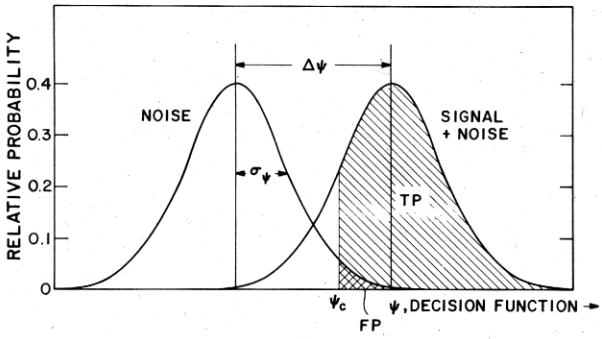

FIG. 3. Probability distributions of the decision function for an image containing pure noise and for an image containing a signal as well as noise. The choice of ψ_c influences the probabilities of true positive (TP) and false positive (FP) responses.

will also be gaussian distributed. Figure 3 shows two probability distributions for ψ, one for images containing only noise and the other for images containing a signal in the presence of the noise. The signal-to-noise ratio SNR, for such a situation is defined as

$$\mathrm{SNR} = \frac{\Delta\psi}{\sigma_\psi}, \tag{30}$$

where $\Delta\psi$ is the difference in the mean values of ψ for the two cases and σ_ψ is the rms deviation of each distribution. The SNR for the binary decision problem at hand is identical with the detection sensitivity index d' used elsewhere.[20]

A threshold ψ_c must be selected in order to make the decision. A positive decision is made (that the object is present) of $\psi \geq \psi_c$ and a negative decision if $\psi < \psi_c$. From Fig. 3 it is clear that a positive decision will be made for certain fraction of images that do not actually contain the object. This is called the "false positive" probability and is represented by the area labeled *FP* in Fig. 3. Similarly the "true positive" probability is labelled *TP*. As ψ_c is varied, TP and FP will also vary and the resulting plot of TP versus FP is called the receiver operating characteristic (ROC) curve.[24] The appropriate choice of the value of ψ_c will depend upon such factors as the relative cost of falsely identifying the presence of the object compared to the cost of missing an object that is present.

From the foregoing discussion it should be clear that the best detection performance is attained when the SNR is maximized. The optimum receiver is that decision criterion which produces the maximum SNR for a given type of noise. In principle, the noise characteristics must be taken into account in the formulation of the decision function ψ to obtain the optimum receiver. If the noise characteristics in the image are different from that assumed in the formulation of the receiver, the receiver may not be optimum. Wagner[6] has derived the SNR of an image for a receiver that is optimized for white (uncorrelated), gaussian noise:

$$\mathrm{SNR}^w = \frac{\iint df_x\, df_y\, |R(f_x,f_y)|^2}{[\iint df_x\, df_y\, S(f_x,f_y)|R(f_x,f_y)|^2]^{1/2}}, \tag{31}$$

where R is the Fourier transform of the object to be detected. It is observed that the signal power as well as its overlap with the noise power spectrum determine SNR^w. One may conclude that for large area objects, it is the behavior of S near zero frequency which dominates the SNR since R^2 will be concentrated there. It is important to emphasize that although S may be arbitrary, Eq. (31) gives the SNR of a receiver optimized for white (S = constant) noise and hence may not be the maximum SNR achievable.

We may now apply signal detection theory to computed tomography. First consider the SNR for the detection of an object using the projection data. It is assumed that m equally spaced projections covering from 0 to π have been taken each with the same white noise spectrum given by Eq. (6). Then using the one-dimensional equivalent of Eq. (31), the SNR for the projection data is

$$\mathrm{SNR}_p^w = \frac{\sum\int df\, |P_j(f)|^2}{[\sum\int df\, S_p(f)|P_j(f)\,|^2]^{1/2}} = \frac{1}{\sigma_p\sqrt{a}}\,[\sum\int df\, |P_j(f)|^2]^{1/2}, \tag{32}$$

where P_j is the Fourier transform of the jth projection of the object and the sums are over all projections from $j = 1$ to m.

The projection-slice theorem states that P_j is identical to the two-dimensional Fourier transform of that object, R, evaluated along a slice through zero frequency at the angle corresponding to the projection:

$$P_j(f) = R(f,\theta_j). \tag{33}$$

Furthermore, in the limit as $m \to \infty$, the summations may be replaced by an integral and the symmetry of the Fourier transform may be used to obtain

$$\mathrm{SNR}_p^w = \frac{1}{\sigma_p}\sqrt{\frac{m}{\pi a}}\left[\int_0^{2\pi} d\theta \int_0^{f_N} df\, |R(f,\theta)|^2\right]^{1/2}. \tag{34}$$

Since the noise in the projections is assumed to be white, this is the optimum SNR for the projection data.

The SNR for the detection of the object in the reconstructed CT image may be readily obtained from Eqs. (4) and (31),

$$\mathrm{SNR}_r^w = \frac{\int_0^{2\pi} d\theta \int_0^{f_N} df\, f\, |R(f,\theta)|^2}{\left[\frac{a\pi\sigma_p^2}{m}\int_0^{2\pi} d\theta \int_0^{f_N} df\, f^2\, |R(f,\theta)|^2\right]^{1/2}} \tag{35}$$

in which we have assumed that $H = 1$, appropriate for the "exact" reconstruction in continuous variables. Since the CT noise power spectrum is not white, SNR_r^w is not the optimum SRN for the reconstruction image. Indeed, it may be shown by simple rearrangement of the moment inequality

$$\langle (f-\bar{f})^2\rangle = \langle f^2\rangle - \langle f\rangle^2 \geq 0, \tag{36}$$

where $\langle\ \rangle$ is the mean value weighted by $|R|^2$ and $\bar{f} = \langle f\rangle$, that

$$\mathrm{SNR}_p^w \geq \mathrm{SNR}_r^w. \tag{37}$$

This is not surprising since SNR_p^w is optimum, whereas SNR_r^w is not. Equation (37) shows that a decision based on the reconstruction which assumes the noise to be white may lead to a smaller SNR than if the decision were based on the projections.

The SNR for an optimum receiver may be obtained from Eq. (31) by "whitening" the noise spectrum so that the resulting spectrum is in agreement with the assumed white noise spectrum. This is done by applying the filter $S^{-1/2}$ to the image. Both R^2 and S are then multiplied by S^{-1} yielding the optimum SNR for the well-known "matched filter" technique[25]:

$$\mathrm{SNR}^0 = \left[\int df_x\, df_y \frac{|R(f_x,f_y)|^2}{S(f_x,f_y)}\right]^{1/2}. \tag{38}$$

The optimum SNR for the reconstruction is

$$\mathrm{SNR}_r^0 = \frac{1}{\sigma_p}\sqrt{\frac{m}{\pi a}}\left[\int_0^{2\pi} d\theta \int_0^{f_N} df\, |R(f,\theta)|^2\right]^{1/2} \tag{39}$$

The result is that for continuous variables there is no loss in the optimum SNR incurred by the process of "exact" reconstruction. Conversely, Eq. (39) implies that in principle, detection performance is not improved by the process of reconstruction.

In the practical case of reconstruction onto a discrete pixel array from discretely sampled projections, there may well be some loss of information. A measure of the amount of information lost in the process of reconstruction is the detective quantum efficiency (DQE)[17]:

$$\mathrm{DQE} = \left[\frac{\mathrm{SNR}_r^0}{\mathrm{SNR}_p^w}\right]^2. \tag{40}$$

Equation (40) may be used to calculate the DQE for any reconstruction algorithm applied to a given object once the optimum SNR's are obtained for the reconstruction and the projection data. An extension to this approach is to define DQE as a function of frequency which avoids the dependence of DQE upon a specific object.

It is readily apparent that "binning" (the discrete representation of the reconstruction), could play a significant role in the detection of small objects, especially when the pixel size is not much smaller than the "spatial resolution." When binning is important, its effect should be taken into account in the calculation of SNR by averaging over all possible positions of the object relative to the display array. If the binning effects are large enough to produce nongaussian ψ distributions (Fig. 3) the simple concept of SNR may not be valid. Rather, the system response characteristics may only be completely described in terms of the ψ distribution or the ROC curves. However, such considerations are unnecessary in the present discussion where our major concern is the detection of large objects.

There is a strong similarity between the SNR for a receiver optimized for white noise, Eq. (32), and the noise granularity relation, Eq. (22). If we define the effective area of the object $r(x,y)$, assumed to be of one sign as

$$A = \frac{[\iint dxdy\, r(x,y)]^2}{\iint dxdy\, r^2(x,y)}, \tag{41}$$

which is consistent with Eq. (20), and its effective contrast ($\Delta\mu$ for x-ray reconstructions) as

$$C = \frac{1}{A}\iint dxdy\, r(x,y), \tag{42}$$

then it is easily shown that the SNR for the reconstruction of objects large enough to be unaffected by the MTF is

$$\mathrm{SNR}_r^w = \frac{C\sqrt{A}}{G}, \tag{43}$$

where G is evaluated with the weighting function

$$w(x,y) = \frac{r(x,y)}{C}, \tag{44}$$

While Eq. 43 provides a useful interpretation of G in terms of SNR_r^w, it should be borne in mind that the latter is not the optimum SNR.

The optimum SNR for the reconstruction of large objects, Eq. 39, may be expressed in terms of the number of equivalent quanta, Eq. 12, as

$$\mathrm{SNR}_r^0 = \left[\frac{\mathrm{NEQ}}{\pi}\int_0^{2\pi} d\theta \int_0^{f_N} df\, |R(f,\theta)|^2\right]^{1/2}. \tag{45}$$

For a gaussian object,

$$r(x,y) = 2C\, e^{-(x^2+y^2)/2\sigma^2}, \tag{46}$$

in the limit as $f_N \to \infty$ (valid for $A \gg$ pixel area, i.e., $A \gtrsim 20$ pixels), this optimum SNR may be expressed as

$$\mathrm{SNR}_r^0 = CA^{3/4}\sqrt{\mathrm{NEQ}}, \tag{47}$$

where $A = 4\pi\sigma^2$. Equation (47) is a good approximation for a large class of objects. For example, the optimum SNR for large circular objects is only 2.1% less than that given by Eq. (47). The nearly universal applicability of Eq. (47) arises from the fact that the optimum SNR for the detection of large objects is mainly dependent upon the slope of S at low frequencies, characterized here by NEQ. It is also noted that the ramplike nature of S leads to an $A^{3/4}$ dependence for the SNR. For white noise (S = constant), the optimum SNR would behave as $A^{1/2}$.

It is interesting to note that Goitein[26] obtained a result comparable to Eq. (47) for the least squares reconstruction algorithm.

The relation between the optimum SNR and G for a gaussian object is obtained using Eq. (29),

$$\mathrm{SNR}_r^0 = 1.253\frac{C\sqrt{A}}{G(A)}. \tag{48}$$

This shows the same dependence as the non-optimum SNR, Eq. (43), but is 25% greater. Equation (48) will be a good approximation for most large objects of area A provided $G(A)$ is obtained using a weighting function with soft edges such as the pyramidal function discussed in Sec. III.

V. APPLICATION TO SCANNER COMPARISON

In the preceding section it has been shown that the slope of S near zero frequency is closely related to the optimum SNR for the detection of large-area, low-density objects in CT images. As a measure of the detectability of such objects, we propose the use of the number of equivalent quanta (NEQ), defined in Eq. (14). The ratio of NEQ to the appropriate measure of dose will then be a suitable figure-of-merit of dose utilization.

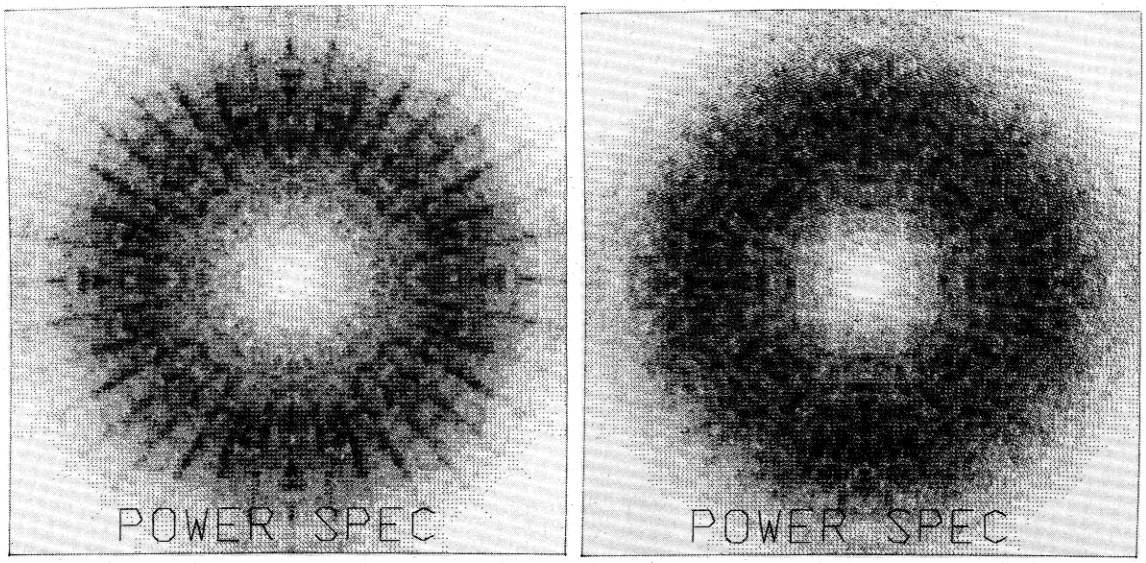

(a) (b)

FIG. 4. Two-dimensional display of noise power spectrum from EMI 5005 (a) before and (b) after recalibration procedure.

The implementation of these concepts will be demonstrated for an EMI CT-5005 x-ray scanner.[27] Six reconstructions of EMI's 10-in. water calibration phantom were used in the following analysis. This phantom consists of a ⅜-in. thick Plexiglas cylinder with a 24-cm inside diameter filled with water. The EMI CT-5005 was operated at 140 KVp in the normal 20-s scan mode. The 320 × 320 reconstruction matrix was obtained by decoding the EMI magnetic tape. Therefore, the results do not include the effects of the normal EMI display device. The pixel width is 0.75 mm.

It was verified that the standard deviation of the noise in each image was constant throughout the image to very high accuracy. Furthermore, the mean values in the reconstruction were quite uniform. For example, the mean value inside a 160 × 160 array in the middle of reconstruction differed from that outside the square and inside a circle of 256 pixels diameter by only 0.17 CT numbers or 0.034%. The almost complete lack of a cusping artifact was presumably due to the fact that these scans were performed on the very phantom used to calibrate the scanner.

The noise power spectral density (S) was estimated from the 6 water scan images using the technique described in the Appendix for $L = 128$ and $N_{aug} = 128$. Only the central 300 × 300 pixels were used. Nine overlapping samples were obtained from each image. Contributions from frequencies below 0.018 mm^{-1} were removed to avoid a bump at $f = 0$. The usefulness of the two-dimensional display of S for diagnosing instrumental problems is demonstrated in Fig. 4. S obtained for the second scan in the series, [Fig. 4(a)] shows enhanced noise along spokes through the origin (center of display). These spokes occur at 10° intervals which is the same as the increment of the scanner angle between translation scans. They may well be caused by the miscalibration of one or several of the 30 detectors used in the EMI CT-5005. Indeed, these spokes disappeared on scans subsequent to the calibration procedure [Fig. 4(b)]. The standard deviation of the noise (σ) changed only slightly, decreasing from about 1.32% before recalibration to 1.28% after.

The radial frequency dependence of S is shown in Fig. 5. S was estimated using all six images which were found to have the same shape. The normalization of S was taken from the scans subsequent to recalibration for which $\sigma = 1.28\%$. S is dimensionless when the reconstruction images are expressed in terms of linear attenuation coefficients ($\mu = 0.190$ cm^{-1} was assumed for water). The curve shown in Fig. 5 was smoothed over a frequency interval of 0.07 mm^{-1} to reduce statistical fluctuations. The estimated uncertainty in the relative values of S varies as $f^{-1/2}$ and is about 1% at $f = 0.35$ mm^{-1}. Recalling the relationship between S and the filter function used in the reconstruction algorithm [Eq. (4)] Fig. 5 shows evidence for a small amount of edge enhancement in the EMI algorithm. While edge enhancement sharpens edges in the image, it usually results in overshoots in the step-response function which are readily observed in EMI CT-5005 reconstructions.

The predicted linearity in S at low frequencies is demonstrated in Fig. 6. The estimates of S at the individual discrete frequencies are presented without smoothing in radial frequency. The only smoothing present is that which results from the use of the Hanning window in the calculation procedure described in the Appendix. Although frequencies below 0.018 mm^{-1} were removed, the point at about 0.012 mm^{-1} is not zero because of this minimal smoothing. The

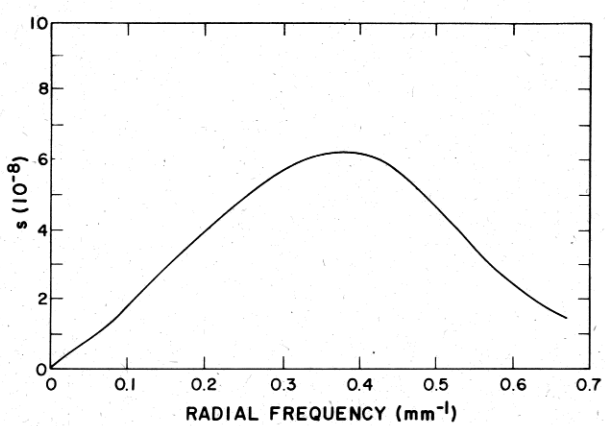

FIG. 5. Noise power spectrum of EMI 5005 scanner used in normal mode with 24-cm-diam reconstruction.

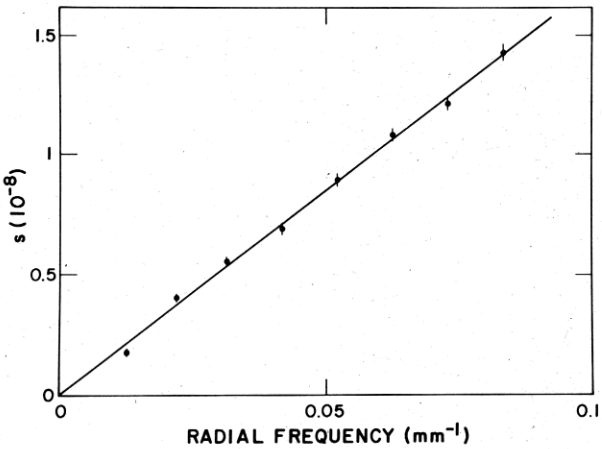

FIG. 6. Low frequency portion of Fig. 5.

error bars shown in Fig. 6 indicate the estimated statistical uncertainty in each datum point. The straight line drawn in Fig. 6 represents the best fit to the data points which passes through the origin. NEQ, determined from the slope of this line using Eq. (14), is $(1.85 \pm 0.03) \times 10^7$ mm^{-1}.

An alternate and less fundamental way to investigate the noise properties is through the noise granularity, G. Figure 7 shows G calculated from the six EMI 5005 water scans using the two weighting functions discussed in Sec. III, square and pyramidal. G was calculated from the rms deviation of the weighted averages taken over non-overlapping square regions. G was normalized to $\sigma = 1.28\%$ as discussed above. It is seen that if the low frequencies are not removed (open triangles, dashed curve), there is a strong effect upon G for large A. Elimination of the frequencies below 0.018 mm^{-1} removes this anomaly. The slope of the pyramidal weighting curve for $\sqrt{A} > 2$ mm is $-\frac{1}{2}$. Thus, for large A, $G \sim A^{-1/4}$, as predicted in Sec. III for CT noises, whereas, for white noise G could be constant. NEQ may be calculated from the normalization of G for large A using Eq. (29) with the numerator equal to 1.240. It is found from the pyramidal curve that NEQ is $(1.81 \pm .05) \times 10^7$ mm^{-1}. This is nearly the same as the NEQ obtained above from the slope of S. The uncertainty in the result is larger than above since nonoverlapping regions were used in the calculation of G and only data within a square completely inscribed within the circle of reconstruction were included. In principle, the same accuracy in NEQ could be attained by either method through complete use of the available data. For comparison, the time required to compute the complete S distribution for the six EMI images was 135 s on a CDC 7600, and the time to compute G at 6 points was 40 s.

As shown in Sec. II, NEQ is the equivalent total number of x-ray quanta detected in all projections per unit length. In the absence of additional noise sources, NEQ is proportional to the dose (D) delivered in the scanning procedure. The NEQ/D ratio is clearly a measure of the efficiency with which the dose is utilized. Since many commercial CT systems provide a selection of slice thickness, this important parameter should be considered. In order to scan contiguous sections, the slices are usually taken at intervals equal to the slice thickness, t. In this situation the dose required to achieve a given NEQ in each slice will be proportional to t^{-1} for a properly collimated x-ray beam. The choice of t might be viewed as similar to the choice of D which must be made on the basis of the diagnostic task at hand. Thus, an appropriate measure of dose efficiency is

$$\zeta = \frac{\text{NEQ}}{D\,t} \tag{49}$$

The dose D may be specified in several ways. Common current practice is to specify the peak surface dose either for a single scan or a series of scans. The surface dose is easiest to measure since the surface is readily accessible. However, the specification of D as the average dose throughout the whole slice for a series of scans has considerable merit. The average dose is appropriate if radiation damage effects are proportional to the integral dose. The integral dose per slice is the average dose times the mass included in one slice. Furthermore, the proportionality of D upon t^{-1} is insured for the average multiscan dose, independent of x-ray collimation. The measurement of the average dose is more difficult since several dose measurements are required over the cross section of the phantom.

Equation (49) suffers from its strong, intrinsic dependence upon the diameter of the phantom. A much more satisfying measure of dose efficiency would be

$$\eta = \frac{D_{\text{NEQ}}}{D}, \tag{50}$$

where D_{NEQ} is the minimum average dose required to produce the measured NEQ for the phantom in question and D is the actual average dose delivered by the scanner. In order for this definition to be useful, D_{NEQ} must be calculated. For a monochromatic x-ray beam of energy E, the average dose for a series of scans is

$$D_{\text{NEQ}} = \frac{E N_{\text{TOT}} \mathcal{F}}{\rho \text{V}}, \tag{51}$$

where N_{TOT} is the total number of incident x rays for each scan, V is the volume of each slice and ρ is the phantom

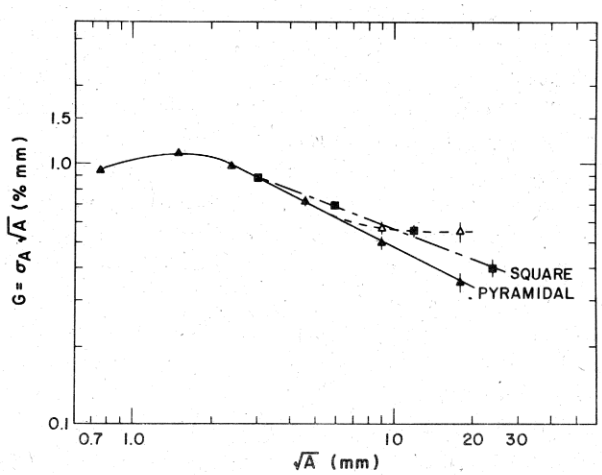

FIG. 7. Noise granularity for EMI-5005 normal scans. The square data points were calculated using constant weight throughout square regions. The triangles result when a pyramidal weighting function is used. The open triangles show the effect of not removing frequencies below 0.018 mm^{-1}.

density. $\mathcal{F}$ is the fraction of the total incident energy that remains in the phantom. For a circular phantom of diameter d, where the incident x-ray beam intensity is varied to keep σ_p (therefore N) constant throughout each projection, Fig. 8,

$$D_{\mathrm{NEQ}} = \frac{4E\ \mathrm{NEQ}\ \mathcal{F}}{\pi\ \rho\ d\ t} I\ (\mu d) \tag{52}$$

where μ is the linear x-ray attenuation coefficient of the phantom at energy E. I is the integral

$$I(\mu d) = \int_0^1 e^{\mu d\sqrt{1-x^2}} dx \tag{53}$$

$$\approx \frac{e^{\mu d}}{\sqrt{\mu d}}\left(1.255 - \frac{0.515}{\mu d}\right). \tag{54}$$

The approximation given in Eq. (54) is accurate to within ½% for $\mu d \geq 2$. The strong dependence of D_{NEQ} upon d is self-evident. Consequently, it is important to state the phantom diameter wherever measurements of NEQ or D are quoted. On the other hand, η should have little dependence upon d. The fraction of energy which is backscattered from the phantom[28] places an upper limit on $\mathcal{F}$ of about 0.75 in the CT diagnostic range of 60 to 100 keV. Furthermore, it is estimated that 10% to 25% of the incident energy will scatter out of the sides or be transmitted through solid phantoms with diameters between 20 and 40 cm. $\mathcal{F}$ is estimated to be approximately 0.6 for a 20-cm-diam phantom and should be a weak function of diameter.

It should be borne in mind that the dose efficiency calculated here is based on a comparison to an ideal CT scanner which employs a monochromatic x-ray beam. All practical scanners are restricted to the use of polychromatic x-ray sources. The utilization of polychromatic x rays leads to a reduction in η for two reasons. The first is that with the light beam filtration often used, a significant portion of the deposited dose arises from low-energy x rays which contribute little to the detected signals (due to enhanced absorption in the phantom). The second reason is that for the detection schemes employed, the detector response is proportional to the integrated energy of the detected x rays rather than to the number of detected x-ray quanta. It is estimated on the basis of primary transmitted x-ray spectra[29] that this typically reduces η by about 10%.

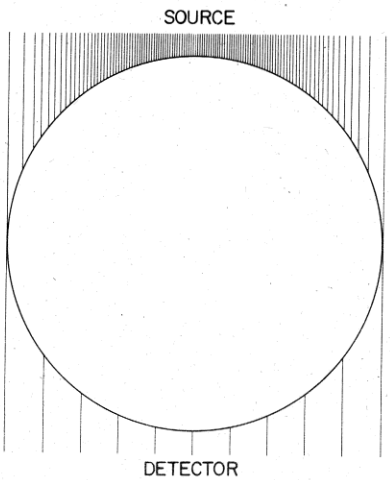

FIG. 8. Idealized x-ray geometry assumed for calculation of D_{NEQ}. The source intensity is reduced at the edges of the phantom to maintain a constant number of unscattered quanta per unit length of detector.

For the EMI CT-5005 the average dose of a normal scan of the 10-in. calibration phantom is estimated to be 3.7 rad for a series of scans taken at 1 cm intervals.[30] Then, using t = 1 cm, Eq. (49) gives $\zeta = 7.12 \times 10^7$ rad^{-1} cm^{-2}. Using E = 82 keV[31], $\mu = 0.182$ cm^{-1},[32] d = 26 cm, and $\mathcal{F} = 0.6$, the dose required by an ideal scanner to achieve NEQ = 1.85×10^7 mm^{-1} is $D_{\mathrm{NEQ}} = 0.43$ rad. Thus, the overall dose efficiency of the EMI CT-5005 is η = 12% compared with the ideal x-ray scanner. It should be noted that this study took place before the scanner was equipped with EMI's dose reducing collimator (No. 5221).

VI. DISCUSSION

There is good evidence that signal detection theory has some applicability to the problem of object detection by the human observer. Numerous studies have been made of the threshold contrast at which human observers are able to detect discs in images containing white noise[33,34] or in "noiseless" images viewed at low light levels.[35] These studies have shown that for objects whose angular subtense at the eye is between 1 and 10 mrad, that the detection threshold of human observers is such as to maintain a constant SNR:

$$\mathrm{SNR}_{\mathrm{th}} = k. \tag{55}$$

The observed values of k range between 2 and 5 depending upon the viewing conditions and the detection criteria.[5,33,34] These values are quite reasonable when one considers their predicted ROC performance[22] for the detection of an object that may be positioned in any one of a large number of positions. However, when human observers are asked to detect the presence of bars or lines, the simple SNR approach does not seem to hold.[36]

The relation of SNR to human detection capability in CT images is not yet fully understood. Several psychophysical studies[14,15,37,38] have indicated that under certain circumstances observer detectability of large objects is improved by smoothing CT images. The reason for this improvement is uncertain. Signal detection theory implies that the SNR of an object is not affected by smoothing (or filtering) provided the receiver is optimized for the noise properties both before and after smoothing. The exception to this is when the filter used in smoothing is zero over some range of frequencies where the signal power is nonzero, in which case the SNR decreases as a result of smoothing. It appears that some deficiency in the human observer detection system is overcome by smoothing the CT images. It is possible that the eye cannot "integrate" the noise properly, perhaps because the noise fluctuations are too large or that the human receiver cannot readily optimize itself to the CT noise characteristics. Further psychophysical investigation of these effects may provide a deeper understanding of the human detection receiver.

In Sec. IV we discussed the application of signal detection theory to the detection of a two-dimensional object on a single CT scan. In reality, however, the radiological detection problem is three dimensional in nature. The difficulties in detecting three-dimensional objects in CT scans have long been referred to as "partial volume" effects. In the three-

dimensional extension of Sec. IV, we might refer to these difficulties as "binning" effects, where the bin width is the individual slice thickness, t. To illustrate the problem, consider a sphere of diameter t immersed in a uniform background of slightly different density. If the sphere happened to lie completely within a CT slice, its effective reconstruction density would be less than its actual density due to the partial volume effect. Moreover, if adjacent slices happened to split the sphere in half, its reconstructed density would be reduced further by a factor of two. The SNR in each slice would be half the maximum SNR. It is interesting to note that if the two slices containing the sphere were averaged, the SNR would increase by the factor of $\sqrt{2}$ over either individual slice. It is clear that there exists an optimum slice thickess for the detection of a given size object if the slices are viewed separately. But a major improvement in detectability at a fixed dose can be achieved by performing the CT scans with small slice thickness and then averaging a variable number of them together to maximize the SNR for various-sized objects. The implementation of a display that allows the observer to make full use of the available three-dimensional information remains one of the most important problems in CT imagery. To emphasize the three-dimensional nature of CT scanning, it might be appropriate to include the slice thickness in the definition of NEQ.

In the present paper we have concentrated on the detection limitations imposed by the statistical noise arising from x-ray quantum detection. There are several other sources of noise which could play an important role in the detection problem. Electronic noise in the detectors or subsequent amplifiers, analog-to-digital converters, etc., is an obvious example. This type of noise will simply add to the statistical noise in the projections and be subjected to the same reconstruction processing. If this noise is white, it will not affect the shape of S. Another source of "noise" is that which arises from artifacts produced by the reconstruction process. These may arise from beam hardening, aliasing or a variety of other causes. Sometimes these artifacts produce clearly defined patterns in the reconstruction. But at other times they are essentially masked by the statistical noise. The point of concern is that artifactual noise contains strong correlations which may add coherently leading to false signals. "Structural" noise may also be present in CT scans even though the reconstruction process removes the principal superposition of overlapping structures. Superposition within the slice thickness due to the partial volume effect may lead to a confusing background against which it is difficult to determine the presence of a lesion.

ACKNOWLEDGMENTS

The author would like to acknowledge many enlightening discussions with Robert F. Wagner. Douglas F. Boyd kindly secured the EMI 5005 scans and Peter Berardo and Sandra Zink decoded the resulting magnetic tape. The author is indebted to T. M. Cannon for most of the noise power spectrum program. This work was supported by the U.S. Department of Energy.

APPENDIX: NOISE POWER SPECTRUM ESTIMATION

The procedure used to estimate the noise power spectrum from an image is the two-dimensional extension of the method due to Welch.[39]

(1) The average value within the circle of interest is subtracted from a reconstruction image which contains only noise.

(2) The area outside the circle of interest is filled with zeros, and the image is windowed using a Hanning window as a function of radial distance which drops to zero at the edge of the circle of interest.

(3) The very low frequencies of the complete image are removed by two-dimensional Fourier transform of the image. The entries for the low frequencies are set to zero and the inverse Fourier transform computed. Removal of the very low frequencies eliminates contributions from cusping artifacts and is as important in CT images analysis as it is in film analysis (Wagner 1977).

(4) An $L \times L$ subsample of image is multipled by a two-dimensional Hanning window and augmented with zeros out to $N_{\text{aug}} \times N_{\text{aug}}$.

(5) The square amplitude (power) of the Fourier transform of the subsample is computed.

(6) Steps 4 and 5 are repeated for subsamples which overlap by $L/2$ in both directions. The two-dimensional noise power spectral density estimate is the average of the power spectrum for all such subsamples. For images known (or assumed) to have symmetry, a symmetrization may be performed to improve statistical accuracy. An octagonal symmetrization is frequently employed by the author.

(7) The one-dimensional radial frequency power distribution is obtained by averaging the power for all two-dimensional frequency values that are near each value of radial frequency. The one-dimensional distribution may be smoothed to reduce statistical fluctuations.

[1]G. N. Hounsfield, Br. J. Radiol. **46,** 1016 (1973).
[2]P. F. J. New, W. R. Scott, J. A. Schnur, K. R. Davis, and J. M. Taveras, Radiology **110,** 109 (1974).
[3]S. J. Riederer, N. J. Pelc, and D. A. Chesler, "Statistical Aspects of Computed X-Ray Tomography," presented at the 45th International Conference on Medical Physics, Ottawa, Canada, 1976.
[4]K. M. Hanson and D. F. Boyd, IEEE Trans. Nucl. Sci., **NS-25,** 160 (1978).
[5]R. F. Wagner, Med. Phys. **4,** 279 (1977).
[6]R. F. Wagner, Photogr. Sci. Eng. **22,** 41 (1978).
[7]L. A. Shepp and B. F. Logan, IEEE Trans. Nucl. Sci. **NS-21,** 21 (1974).
[8]E. Tanaka and T. A. Iinuma, Phys. Med. Biol. **20,** 789 (1975).
[9]R. Zacher, *Reconstruction Tomography in Diagnostic Radiology and Nuclear Medicine,* edited by M. M. Ter-Pogossian, *et al.* (University Park, Baltimore, 1977), p. 59.
[10]S. A. Johnson, *Reconstruction Tomography in Diagnostic Radiology and Nuclear Medicine,* edited by M. M. Ter-Pogossian, *et al.* (University Park, Baltimore, 1977), p. 199.
[11]H. H. Barrett, S. K. Gordon, and R. S. Hershel, Comput. Biol. Med. **6,** 307 (1976).
[12]R. A. Brooks and G. DiChiro, Med. Phys. **3,** 237 (1976).
[13]D. A. Chesler, S. J. Riederer, and N. J. Pelc, Comput. Assist. Tomogr. **1,** 64 (1977).
[14]P. M. Joseph, Proc. SPIE **127,** 43 (1977).

[15]K. M. Hanson, Proc. SPIE **127,** 304 (1977).
[16]S. J. Riederer, N. J. Pelc, and D. A. Chesler, Phys. Med. Biol. **23,** 446 (1978).
[17]J. C. Dainty and R. Shaw, *Image Science* (Academic Press, London, 1974).
[18]R. F. Wagner, D. G. Brown, and M. Pastel, "Toward a Measure of the Information/Radiation Ratio in CT," presented at the International Symposium and Course on Computed Tomography, Miami Beach, FL, 1978.
[19]E. W. H. Selwyn, Photgr. J. **75,** 571 (1935).
[20]A. D. Whalen, *Detection of Signals in Noise* (Academic Press, New York, 1971).
[21]H. L. Van Trees, *Detection, Estimation and Modulation Theory* (John Wiley and Sons, New York, 1968).
[22]D. J. Goodenough, Proc. SPIE **47,** 134 (1975).
[23]D. J. Goodenough and C. E. Metz, J. Acout. Soc. Am. **55,** 111 (1974).
[24]D. J. Goodenough, K. Rossman, and L. B. Lusted, Radiology **110,** 89 (1974).
[25]W. M. Brown, *Analysis of Linear Time-Invariant Systems* (McGraw-Hill, NY, 1963).
[26]M. Goitein, Nucl. Instrum. Methods **101,** 509 (1972).
[27]EMI Medical Inc., 4000 Commercial Drive, Northbrook, IL 60052.
[28]M. J. Berger and J. Raso, Radiat. Res. **12,** 20 (1960).
[29]M. M. Ter-Pogossian, et al., Radiology **113,** 515 (1974).
[30]R. C. Brasch, D. P. Boyd, and C. A. Gooding, Am. J. Roentgenol. **131,** 95 (1978). The average dose reported here for an effective diameter of 21 cm was scaled by $(\text{diameter})^{-1}$. It was assumed that the ratio of the dose for the 24-cm scan diameter to that for the 32-cm diameter is inversely proportional to the translation speed, i.e., 1.4.
[31]M. R. Millner, *et al.,* Med. Phys. **5,** 543 (1978).
[32]E. Storm and H. I. Israel, Nucl. Data Tables **A7,** 565 (1970).
[33]F. A. Rosell and R. H. Willson, *Perception of Displayed Information,* edited by L. M. Biberman (Plenum Press, New York, 1973).
[34]A. Rose, J. Opt. Soc. Am. **38,** 196 (1948).
[35]H. R. Blackwell, J. Opt. Soc. Am. **36,** 624 (1946).
[36]A. E. Burgess and K. Humphrey, Proc. SPIE **127,** 51 (1977).
[37]R. A. Brooks, E. Chew, G. H. Weiss, and G. DiChiro, "Effect of CT Noise on Detectability of Test Objects," presented at the International Symposium and Course on Computed Tomography, Miami Beach, FL, 1978.
[38]S. C. Orphanoudakis (private communication).
[39]P. D. Welch, IEEE Trans. Audio Electroacoust. **AU-15,** 70 (1967).